

# HeRe: Heartbeat Signal Reconstruction for Low-Power Millimeter-Wave Radar Based on Deep Learning

Haili Wang<sup>ID</sup>, Fuchuan Du<sup>ID</sup>, Hao Zhu<sup>ID</sup>, Zhuangzhuang Zhang<sup>ID</sup>, Yizhao Wang<sup>ID</sup>, Qixin Cao<sup>ID</sup>, and Xiaoxiao Zhu<sup>ID</sup>

**Abstract**—The noncontact monitoring of vital signs without body-attached sensors is a promising home healthcare technique. Recent studies have shown that millimeter-wave (mmW) radar can be used to continuous daily monitoring of vital signs such as heart rate (HR) and respiratory rate (RR). To minimize disruption to the user's daily life and accommodate for home environments, low-power radar or radar with antennas in package (AiP) is becoming increasingly popular. However, the lower transmitting power of these systems can lead to decreased signal-to-noise ratio (SNR) of the radar signal, making established measurement methods ineffective. The vital signs, particularly HR, are no longer accurately measured due to the small amplitude associated with heartbeats. In this work, we present HeRe for low-power radar, a deep learning (DL) approach for heartbeat signal reconstruction. The proposed method uses a neural network to identify patterns in the signal, leading to a significant improvement in the SNR of the heartbeat signal. By leveraging historical data, the current HR estimation is further refined, yielding improved precision in the results. Experiments have demonstrated the efficacy of signal reconstruction for improving the heartbeat signal in both the time and frequency domains. A comparison of the proposed approach to related works on various HR distributions, sensing ranges, and subjects showed significantly higher accuracy. To further assess the robustness of the proposed approach, extended continuous monitoring was performed and 97.5% accuracy was achieved. This article highlights the advantages of DL techniques for noncontact, radar-based HR monitoring, leading to accurate HR monitoring with the lowest power consumer-grade mmW radar currently available on the market.

**Index Terms**—Deep learning (DL), heart rate (HR), low-power, millimeter-wave (mmW) radar, signal reconstruction, vital signs monitoring.

Manuscript received 2 November 2022; revised 3 February 2023; accepted 19 March 2023. Date of publication 17 April 2023; date of current version 26 April 2023. This work was supported in part by the National Key Research and Development Program of China under Grant 2019YFC1711801. The Associate Editor coordinating the review process was Dr. Kamel Haddadi. (Corresponding author: Xiaoxiao Zhu.)

Haili Wang, Fuchuan Du, Hao Zhu, Zhuangzhuang Zhang, Yizhao Wang, and Qixin Cao are with the State Key Laboratory of Mechanical System and Vibration, Shanghai Jiao Tong University, Shanghai 200240, China (e-mail: sjtu\_wanghaili@sjtu.edu.cn; yunzhongxicao@sjtu.edu.cn; sour123@sjtu.edu.cn; zhangzz616296@163.com; wangyizhao@sjtu.edu.cn; qxcao@sjtu.edu.cn).

Xiaoxiao Zhu is with the State Key Laboratory of Mechanical System and Vibration and the Student Innovation Center, Shanghai Jiao Tong University, Shanghai 200240, China (e-mail: ttl@sjtu.edu.cn).

Digital Object Identifier 10.1109/TIM.2023.3267348

## I. INTRODUCTION

WITH the COVID-19 pandemic, it has become valuable to monitor one's health in own house using new technology. In particular, the vital signs heart rate (HR) and respiratory rate (RR) are crucial for home healthcare and have attracted tremendous attention. Reliable and accurate HR/RR monitoring is a helpful tool for diagnosing cardiovascular disease, assessing sleep quality, etc. Aside from that, continuous monitoring can even facilitate the early detection of functional decline and health deterioration based on the changes in HR/RR over a long period.

For HR monitoring, electro-cardiography (ECG) and photoplethysmography (PPG) devices, which are contact monitoring devices, are still the gold standard for clinically characterizing cardiac activities. Both of them require attaching several self-adhesive electrodes or sensors to the skin of the human body to obtain the high-quality heartbeat signal [1]. However, they are inconvenient and cause discomfort, which can limit their long-term use. In addition, they are unsuitable for individuals with skin allergies and dementia, and the patients' awareness of being monitored can affect the accuracy of the measurements.

Noncontact sensor technology, on the other hand, can estimate HR from a distance without electrodes and touch, making it simpler and more comfortable for use. Generally, it gives a low-cost, high-temporal-resolution way to monitor health conditions anytime and anywhere without any operation. It enables constant, long-term self-monitoring of HR in daily life. Thus, patients from any area are linked to physicians and able to acquire clinical trial data without the necessity for an in-person visit.

In recent years, a noncontact vital signs' monitoring system based on millimeter-wave (mmW) radar has been developed for use in home healthcare. Radar transmitters emit and broadcast electromagnetic signals into space, while the radar receivers record the echoes returned by the human body, which carry the human signature based on different distances, sizes, speeds, and other factors. The fundamental method for estimating HR/RR with radar involves measuring the micro-movement between the antenna and the chest, which is caused by heart-pumping action and respiration.

MmW radar-based monitoring, as one of the noncontact monitoring systems, frees people from discomfort,

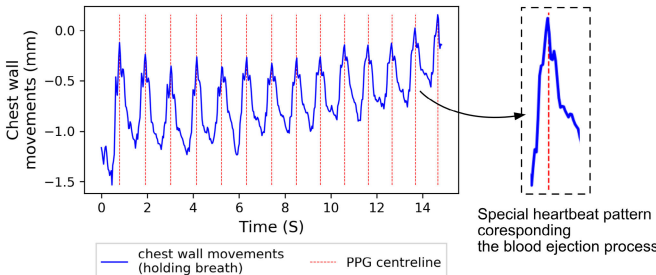


Fig. 1. Chest wall displacement patterns influenced by heartbeat when breath-holding.

increases the acceptable monitoring period, and eliminates biases induced by psychological stress or physical constraints caused by contact measuring equipment. On the other hand, as opposed to the noncontact monitoring approach based on video surveillance systems [2], [3], mmW radar does not rely on visual data. The radar sensors are based on radio frequency (RF) signals and are therefore unaffected by lighting conditions and clothing opacity. No image video signals are generated, so there are no privacy concerns for private housing use. Therefore, radar is well-suited for use in home HR monitoring.

A variety of radars have been used in related works to estimate vital signs remotely, including the continuous-wave (CW) radar [4], [5], the ultrawideband (UWB) radar [6], [7], [8], and the frequency-modulated CW (FMCW) radar [9], [10], [11]. Early in [9], [12], and [13], the feasibility of HR estimation using a radar system is investigated. However, their work focuses on the theoretical foundation and assumes no other nearby noise sources exist. Yang et al. [14] started focusing on solving the practical challenges by finding the human location in a room and estimating the vital signs concurrently. Since the FMCW radar gets not only the Doppler information but also the range information, it is good for distinguishing clutter and multiple targets, making it a mainstream choice in the field of vital signs monitoring.

However, the home environment is filled with various types of furniture and other clutter, and it is still difficult to estimate vital signs with enough accuracy and robustness, especially for HR.

The reason is that the chest wall movements caused by the heartbeat are quite small, and the noise usually is comparable to or even stronger than the weak heartbeat signal. Besides, for a healthy adult, the chest displacement varies between 4 and 12 mm for respiration and 0.2–0.5 mm for the heartbeat. About 0.2–0.34-Hz and 0.9–1.60-Hz frequency variations are observed for RR and HR, respectively [15]. The HR signal is much smaller in amplitude and slightly higher in frequency than the RR signal. However, respiration is not a perfect sinusoidal motion since inhalation and exhalation duration can differ. This creates high-frequency components from the respiration motion that interfere with the micro heartbeat. The second and third-order harmonics of RR signals are still comparable in magnitude to HR fundamental frequency and cause interferences that cannot be filtered easily.

There is quite a long history of studying extracting the component signals from noisy radar raw data, which is

usually mixed from respiration, heartbeat, and noise. Most studies were performed under conditions of high transmitting power, seldom compared in terms of hardware complexity and power consumption even though these aspects are of utmost importance for real applications. However, it is challenging to obtain similar performance with low transmitting power mmW radar, which is more appropriate for use in home environments. In the past few years, the use of low-power mmW radars in living areas is growing in popularity. With a higher frequency and a shorter wavelength, mmW radar antennas can be manufactured in extremely compact sizes, even sharing the same package with the control integrated circuit [i.e., antennas in package (AiP)] as a radar chip. It is possible to embed a miniature, low-power radar chip into the home environment, thus reducing interference with the user's daily life, broadening the deployment of scenarios and places, and enhancing the application value. In recent consumer electronics, Google has used mmW radar in smart speakers [16] to monitor human respiration rate and sleep status and in smartphones for simple gesture interaction [17]. The Aqara company introduces FP1, a low-power mmW radar human presence sensor that enables the detection of static human bodies, which are not distinguishable by conventional PIR [18].

Unfortunately, there are few applications of low transmit power radar in HR estimation in the related literature. From the perspective of the radar hardware platform used, some laboratory-based studies used custom-built radar systems [11], [19], [20], [21], which achieved higher transmitting power and signal-to-noise ratio (SNR) using a directional horn antenna with a relatively high gain. However, this approach is not conducive to promotion due to increased hardware cost. With the advent of integrated mmW radar modules, more studies have adopted commercially available consumer mmW radars [10], [22], [23], [24], [25], [26], [27]. The directional gain antenna is no longer used and the antenna area is reduced by integrating the antenna onto the PCB board, making multi-input–multi-output (MIMO) technology also easier to implement. The transmitting power has dropped to around 13 dBm to meet regulatory requirements for indoor radar use [28]. The rise in low-power mmW radar use and mature of AiP technology has led to a few studies, which attempted HR monitoring using low-power radar chips. Due to the cost of extra attenuation with the distance, which lowers the signal SNR, the monitoring distance in these studies is generally short (within 0.5 m) and it is difficult to ensure accurate HR monitoring capability [29], [30], [31], [32].

From the perspective of used signal processing algorithms, most methods proposed by related works could be categorized into four groups: Spectrum analysis methods, nonstationary decomposition methods, complex signal processing methods, and deep learning (DL)-based methods. The spectrum analysis methods are based on frequency and amplitude analysis in the frequency domain. Many early proposals relied on Fourier transform analysis [10], [19], [22], [23] and wavelet transform [20], [31] followed by bandpass filtering (BPF) to extract frequency information related to heart beats. These methods apply fast Fourier transform (FFT) and BPF to separate the

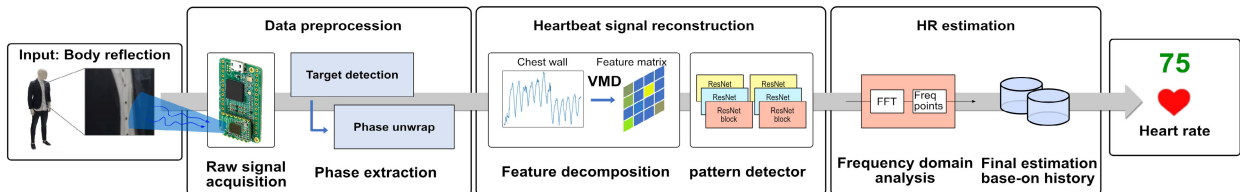


Fig. 2. Overview of the HR monitoring system based on HeRe for low-power mmW radar.

heartbeat signals and find the largest spectral values in the bands as the corresponding estimated HR. However, these methods struggle to distinguish noise with frequencies similar to heart beats, which is commonly encountered in real-world applications. The wavelet method used the multiresolution analysis using continuous wavelet transform. The periodicity in a specific frequency is extracted, which infers the heartbeat. Therefore, noisy harmonic components could be eliminated. To further enhance the strength of the heartbeat signal in spectrum, special differential operators (DE) [11], [33] were considered as a preprocessing step for mixed signals, designed based on prior knowledge of the signals. The customized differential operators that have higher gain on special frequency signals and the enhancement on the heartbeat corresponding component make it easier to estimate the HR value. However, generalizing the parameters of these differential operators to different devices and situations is still a challenge. In the category of nonstationary decomposition methods, there exist techniques for processing nonlinear nonstationary signals. Two examples of such methods are empirical mode decomposition (EMD) [24], [34] and variational mode decomposition (VMD) [21], [27], which have been utilized as blind source separation algorithms for extracting vital sign signals from noise. Due to the mode-mixing phenomenon in the application of the EMD method, the latter ensemble EMD (EEMD) and VMD-based methods are proposed to address this issue and improve the confidence of the actual decomposition results. Nonetheless, extracting the heartbeat signal remains challenging due to overlapping frequency ranges and the presence of harmonics with normal respiration. Other methods can be classified as advanced signal processing methods, which do not use traditional signal decomposition and spectral analysis approaches, but instead incorporate recent developments in the field of signal processing, such as compressive sensing, state estimation, and time-frequency joint analysis. The work of [25] proposed a compressive sensing-based orthogonal matching pursuit (CS-OMP) algorithm for reconstructing heartbeat signals and suppressing respiration harmonic interference and noise. This approach achieves more precise signal reconstruction with lower sampling costs, even in the presence of noise. In other works [35] and [30], an integrated time-frequency-domain analysis method was used to optimize the HR estimation results by limiting and filtering the data, and counting the number of peaks in the time-domain signal to select the correct frequency in the spectrum. The work [29] proposed the use of a Kalman filter to track and limit the frequency range of the search for HR, to avoid sudden misalignments caused by noise. However, these methods still have the basic requirement for quality signals and do not fundamentally improve the SNR of the signal, and therefore do

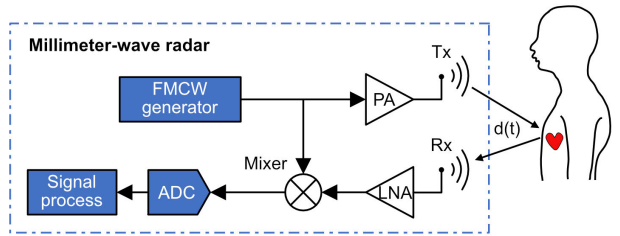


Fig. 3. Block diagram FMCW of the mmW radar HR monitoring system.

not achieve good accuracy under low-power radar conditions. Vodai et al. [26] and Sakamoto and Yamashita [36] proposed the use of maximal ratio combining (MRC) to synthesize multiple signals from an MIMO system and improve the SNR. However, this technique requires a large number of virtual signals, which results in increased cost and difficulty for daily use (e.g., even 12 transmitters with 16 receivers—192 virtual signal channels are used). Meanwhile, recently some works have used machine learning approaches in HR monitoring, categorized as DL-based methods. For instance, the end-to-end model (mBeats) proposed in [37], which formulates HR estimation as a regression problem and uses a convolutional neural network. However, due to the low power of the radar and the low SNR of the signal, these methods may lead to overfitting and poor performance in practical application. Mauro et al. [32] proposed the use of meta-learning (Meta-L) to improve the generalization ability of the network model, but this work only focused on monitoring breathing frequency. Currently, there is no mature, DL-based, low-power mmW radar HR monitoring work that is targeted toward practical applications.

The related works have been systematically reviewed and tabulated in Table I in accordance with their transmission power and publication date. The table includes information about the radar platform, the primary method used, the sensing range, and the relevant performance parameters. However, due to the absence of a standard dataset and the corresponding evaluation criteria in this research field, the performance of each work is represented based on the evaluation criteria used in the respective article. Information that is not provided is indicated with “-.”

Low SNR of the low-power mmW radar makes it difficult to obtain reliable HR estimates in practical uses, and it has become the primary barrier to the widespread application of HR monitoring mmW radar devices in home.

Previous works have focused on the frequency and amplitude characteristics of the signal, whereby the target human's heartbeat signal is extracted from the noisy signal. However, under low SNR conditions, these methods suffer from noise

TABLE I  
CURRENT STATUS OF THE RESEARCH ON MMW RADAR HR MONITORING

Related works	Radar platform	Method	Transmitting power (dBm)	Range (m)	Performance parameter
Sekine, 2011 [20]	NJR4261J	Wavelet	38.5	1.0	92.5% Accuracy
Wang, 2021 [35]	PEM009	TFiHR	25-39	1-7	1.5BPM Error
Matthews, 2000 [19]	Non-consumer radar	FT+BPF	20.1	-	-
Xiong, 2020 [11]	Non-consumer radar	DE	17	1.5	100% with error of less than 5%
Lee, 2019 [23]	IVS-162	MUSIC+FFT+BPF	15	3.0	96.20% Accuracy
Vodai, 2021 [26]	AWR2243	Wavelet+MRC	13	1.7	0.1BPM RMSE
Wang, 2020 [25]	AWR1642	CS-OMP	12.5	0.9	4.38BPM RMSE
Ding, 2017 [21]	NVA6100	VMD	12	1.5	-
Weishaupt, 2018 [34]	Non-consumer radar	EMD	-	-	6.0BPM Error
Alizadeh, 2019 [10]	AWR1443	FFT+BPF	12	1.7	80% Accuracy
Huang, 2019 [22]	IWR1443	MIMO+FFT+BPF	12	0.7	-
Sun, 2020 [24]	IWR1642	Adaptive identification embedded EEMD	12	2.5	4.75BPM RMSE
Zhao, 2020 [37]	IWR6843	End-to-end DL	12	0.5	92.0% Accuracy
Zhang, 2022 [27]	IWR1443 with IWR1642	IMCA+APVMD	12	1.0	1.15BPM Error
Arsalan, 2020 [29]	BGT60TR13C	BPF+Kalman filter	6	0.4	7.0 RMSE
Zhang, 2022 [30]	BGT60TR13C	Coarse-to-fine estimation	6	1.5	85.6% with error of less 4BPM
Chanhee, 2022 [31]	BGT60TR13C	Wavelet	6	-	-
Mauro, 2023 [32]	BGT60TR13C	VAE+Meta L	6	0.3-0.4	-

with larger magnitudes and closer frequencies to that of heartbeat signals, making it challenging to obtain the desired accuracy. However, the chest wall movement due to the heartbeat is generated by the blood ejection process by the heart [38]. Therefore, the movement should have a fixed pattern. By holding the body still and holding breath, we observed distinct heartbeat signals with a particular pattern in the chest wall movement signal obtained by radar, as shown in Fig. 1. Inspired by some recent excellent studies in the field of computer vision, we consider using a deep neural network to detect this particular pattern better, as they have been validated in many domains for complex classification, detection tasks.

In this article, to recover reliable HR parameters from low SNR radar signal, a DL-based HR estimation method for low-power mmW radar is proposed.

Unlike other works, the proposed method interprets the heartbeats as pulse signals. A sliding window is used over the chest wall movement stream feeding the windowed frames to a neural detector concentrating heartbeat pulse. Using the detected frequency of the heartbeat as the HR equivalent, the signal reconstruction process is achieved by signal pattern detection. The VMD algorithm exploits the different central-frequency components to assess better whether the present frames correspond to heartbeats. It converts the 1-D time series into a 2-D matrix. Finally, a high-precision frequency estimation will be performed, using the historical data.

The main advantages of our approach compared with the existing works are as follows.

- 1) The deep neural-network-based detector successfully detects heartbeats with high accuracy in low SNR radar data. The time series of detection results are treated as a reconstructed heartbeat signal for continuous HR monitoring.
- 2) The VMD algorithm is introduced to provide information on the different frequency components of the signal, offering a richer input feature for the detection network and enhancing the network's monitoring efficiency.
- 3) The effectiveness of using a deep neural network detector to reconstruct the heartbeat signal is analyzed in the time and frequency domains. The proposed method is compared with other non-neural-network-based methods

to highlight the advantages of the proposed method in real scenario monitoring.

The rest of this article is organized as follows. In Section II, the radar signal collection and preprocessing are described. Meanwhile, the proposed method HeRe, including signal reconstruction and HR estimation, is provided in detail. Then, the experiments and evaluations are presented in Section III. Finally, Section IV concludes the article.

## II. METHODS

Fig. 2 shows the scheme of the HeRe. The proposed HeRe method consists of three steps: data preprocessing, heartbeat signal reconstruction, and HR estimation.

- 1) *Data Preprocessing*: Intermediate frequency signal (IF signal) and range–Doppler matrix are obtained from the raw received signal. Then, the range corresponding to the target human body is identified, and the micro-movement signal at the target range bin is extracted as the input signal to the following reconstruction process.
- 2) *Heartbeat Signal Reconstruction*: The extracted 1-D micro-movement signal is decomposed into a 2-D feature matrix by the VMD algorithm, and the sliding window moves and samples the feature matrix to create a dataset. The dataset is passed to the detector network to identify the presence of a heartbeat signal.
- 3) *HR Estimation*: After performing the detector network, the challenge of obtaining high-accuracy HR value remains. A frequency-domain analysis with historical data correction is applied to obtain high-accuracy HR estimation.

### A. Data Preprocessing

The mmW radars can be divided into various radars according to their transmit waveforms. The radar used in the project are frequency-modulated CWs (FMCWs), which means the frequency of the emitted waveforms sweeps linearly from the start frequency  $f_{\min}$  to the end frequency  $f_{\max}$  in the duration of  $T_r$  (also named as fast time). The sweeping bandwidth  $B = f_{\max} - f_{\min} = KT_r$ , where  $K$  is the slope of frequency of Tx signal.

Unlike typical Doppler radar, FMCW radar not only provides target Doppler information (velocity information) but also targets range information at the same time. They can distinguish targets with clutters in different ranges and extract targets' micro-movement information, making it a mainstream choice in the field of vital detection indoor.

As represented in Fig. 3, the transmitted wave is generated through the waveform generator and modulated through the voltage control oscillator (VCO). After that, the transmitted signal is amplified by a power amplifier (PA) and sent to the external environment through the Tx antenna. After reflecting by the target within the monitoring range, the wave is received by the Rx antenna and passed through a low-noise amplifier (LNA) to obtain a signal of the same frequency as the transmitted signal. The FMCW radar system measures distance and velocity via the IF signal  $s_{if}(t)$ , which is the difference between the transmitted and received signals.

The complex transmitted signal is

$$s(t) = A_t \exp(j(2\pi f_{min} t + \pi K t^2)), \quad 0 < t < T_r. \quad (1)$$

The received signal is a delayed version of  $s(t)$  with a delay of  $t_d = 2d(t)/c$ , where  $c$  stands for the velocity of light, and  $t_d$  stands the range of the target chest wall relative to the radar.  $d(t)$  consists of three components as follows:

$$d(t) = d_0 + x(t) = d_0 + d_R + d_H \quad (2)$$

where  $d_0$  is the average range of the human chest wall relative to the radar, which can be regarded as constant when the human body is held steady.  $x(t) = d_R + d_H$  are the micro-movement of the chest wall caused by respiration and heartbeat, respectively.

Consequently, the RX signal and the TX signal are passed to the mixer to obtain the IF signal  $s_{if}(t)$

$$\begin{aligned} s_{if}(t) &= A_t A_r \exp(j(2\pi f_{min} t_d + 2\pi K t_d t - \pi K t_d^2)) \\ &\approx A_t A_r \exp(j(\psi(t) + \omega_b t)), \quad t_d < t < T_r \end{aligned} \quad (3)$$

where  $\psi(t) = 4\pi((R_0 + x(t))/\lambda)$ ,  $\omega_b \approx 4\pi(K R_0/c)$ .

The approximate result  $\omega_b$  is obtained after ignoring the micro-movement  $d_R$  and  $d_H$  terms, because  $T_r < 1$  ms and the micro-movement is almost constant within single transmit duration  $T_r$ .  $\lambda$  is the wavelength of the radar waveform, which equals 5 mm for 60-GHz radar, for instance.

According to (3), the IF signal is approximated into a sinusoid signal in which the angular frequency and the phase are equal to  $\omega_b$  and  $\psi(t)$ , respectively.

FFT is applied to the samples of the IF signal. The output spectrum has peaks corresponding to the subjects at different ranges. So it is called the range FFT.

Each range FFT bin represents a particular range with an associated phase similar to  $\psi(t)$ . For measuring the time-varying heartbeat signal, multiple Tx signals are sent in a sequence, which is equivalent to the sampling of  $x(t)$ . Micro-movement of the chest wall  $x(t)$  is sampled each  $T_c$  ( $T_c \geq T_r$ ), also known as slow time.

As shown in Fig. 4, we form IF signal  $s_{if}(t)$  into a matrix, and then perform FFT to obtain the range-slow time matrix  $M(r, a, t)$  (also known as the range-Doppler matrix), in which

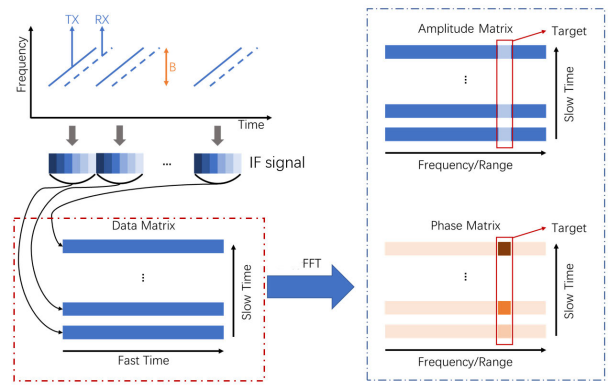


Fig. 4. IF signal generation range-slow time matrix process.

$r$ ,  $a$ , and  $t$  represent the range, amplitude, and slow time, respectively. Therefore, the amplitude information of heartbeat and breath can be obtained by extracting the phase from the range FFT bin corresponding to the target range.

Moreover, to obtain the accuracy range of the target, it is necessary to eliminate the interference of static clutters. The echo signal contains static clutter from the reflections of floors, walls, and other static objects in the environment. These background noises can lead to extremely large reflection components, which can bias the judgment of range. One general method of the traditional radar technology called moving target indicator (MTI) is used in this article. This method regards the time-average intensity of each pixel in the range-slow time matrix as the background noise. Then the echo signal from clutters could be subtracted from the range-slow time matrix  $M(r, a, t)$

$$\begin{aligned} M(r, a, t)_{clutter} &= \frac{1}{k} \sum_{i=t-k}^{t-1} M(r, a, i) \\ M(r, a, t)_{MTI} &= s - \alpha M(r, a, t)_{clutter} \end{aligned} \quad (4)$$

where  $M(r, a, t)_{MTI}$  notes the denoised range-slow time matrix, and  $\alpha$  is an intensity parameter.

Fig. 5 depicts the MTI method's effects. The entire matrix was highly chaotic before the MTI method was used [as Fig. 5(a)], and it was hard to measure the position of the human body. On the contrary, the periodic peaks can clearly be observed at the true position of 1 m after MTI [as Fig. 5(b)].

Due to the periodicity of the phase, the phase values obtained are restricted to the values of  $(-\pi, \pi]$ , a phenomenon known as phase wrap. However, the actual phase can change beyond  $2\pi$  when the physical displacement is greater than the wavelength, for instance,  $\lambda = 5$  mm of the 60-GHz radar. Therefore, phase unwrapping is a necessary process to ensure proper phase extraction. The simple procedure discussed in [10] is performed on the phase series.

The chest wall micro-movement phase series is obtained through the above signal preprocessing, which will be passed to the following reconstruction process.

#### B. Heartbeat Signal Reconstruction

In the past work, researchers have generally treated both respiration and heartbeat as equivalent to the typical sinusoidal-

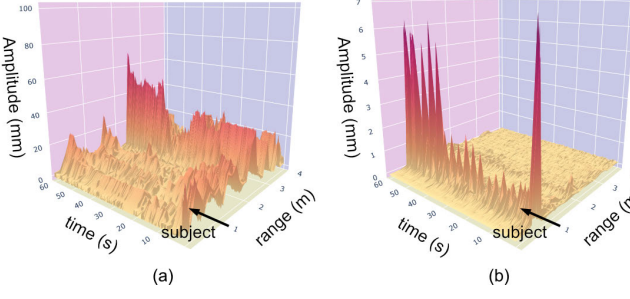


Fig. 5. MTI method's clutter suppression effects. Range–slow time matrix (a) before and (b) after MTI.

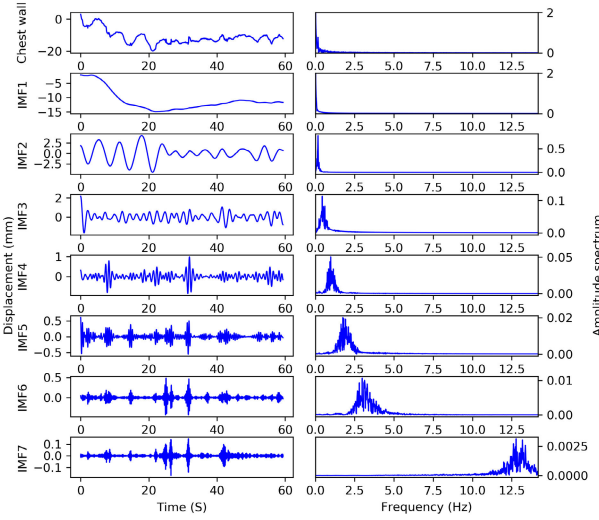


Fig. 6. Chest wall displacement decomposed by the VMD algorithm.

like signal, differing only in its periodicity and amplitude. However, in fact, there is a clearly recognizable signal pattern with each heartbeat time, which has a stronger resemblance to the periodic pulse signal (as shown in Fig. 1). We propose to treat the heartbeat signal as a pulse signal instead of the traditional periodic sinusoidal signal based on the analysis of the waveform pattern. Our method transforms the problem of signal reconstruction into a signal pattern detection problem using a sliding window over the received radar signal. The windowed frames are continuously fed to a neural detector, which labels the frames as either “heartbeat” or “non-heartbeat.” The focus is on the frequency characteristics of the heartbeat, as the goal is to obtain the HR. The result sequence of the detection process possesses the same periodicity and spectrum distribution as the original heartbeat signal and is able to eliminate noise or distortion not related to the heartbeat, thanks to the power of deep neural networks. Thus, the signal pattern detection result sequence serves as the reconstructed heartbeat signal and can be used for further estimation of the HR.

In the feature extracting part, to exploit the different frequency components of the radar signal that can be fully used, the VMD method [39] was used to first decompose the original signal with independent frequency components.

TABLE II  
LAYER ARCHITECTURE OF THE PROPOSED DETECTOR NETWORK

Layer name	Output size	Kernel
Conv layer	$7 \times 72$	$3 \times 3$ conv, 64 $3 \times 3$ max pool
Residual layer1	$7 \times 72$	$\begin{bmatrix} 3 \times 3, 64 \\ 3 \times 3, 64 \end{bmatrix} \times 2$
Residual layer2	$4 \times 36$	$\begin{bmatrix} 3 \times 3, 128 \\ 3 \times 3, 128 \end{bmatrix} \times 2$
Fc layer	$1 \times 1$	$2 \times 2$ avg pool fc, softmax

The VMD algorithm is an entirely nonrecursive VMD method, and the modes are extracted concurrently. The recovered VMD modes called intrinsic modal component (IMF) realize an effective separation of the signal from low frequency to high frequency.

First, construct a variational problem, assuming that each mode is a finite bandwidth with a center frequency

$$\begin{aligned} \min_{\{u_k\}, \{\omega_k\}} & \left\{ \sum_{i=1}^K \left\| \partial_t \left[ \left( \delta(t) + \frac{j}{\pi t} \right) * u_k(t) \right] e^{-j\omega_k t} \right\|_2^2 \right\} \\ \text{s.t. } & \sum_{k=1}^K u_k = x_f(t) \end{aligned} \quad (5)$$

where  $k$  is the number of IMF to be recovered,  $u_k$  is the  $k$ th IMF,  $\omega_k$  is the  $k$ th center frequency, and  $x_f(t)$  is the mirror-symmetric extension of the original chest wall displacement.

Then the quadratic penalty function and Lagrange multipliers are used to solve the following constructed variational equation:

$$\begin{aligned} \mathcal{L}(\{u_k\}, \{\omega_k\}, \lambda) &:= \alpha \sum_k \left\| \partial_t \left[ \left( \delta(t) + \frac{j}{\pi t} \right) * u_k(t) \right] e^{-j\omega_k t} \right\|_2^2 \\ &+ \left\| x_f(t) - \sum_k u_k(t) \right\|_2^2 + \left\langle \lambda(t), x_f(t) - \sum_k u_k(t) \right\rangle \end{aligned} \quad (6)$$

where  $\alpha$  represents the balancing parameter of the data-fidelity constraint, which is clearly identified as a Wiener filtering of the current residual, with signal prior  $1/(\omega - \omega_k)^2$

The alternate direction method of multipliers (ADMM) [40] is used to obtain all IMFs in the  $n$ th cycle using the following formulas:

$$\hat{\mu}_k^{n+1} = \frac{\hat{x}_f(\omega) - \sum_{i \neq k} \hat{\mu}_i(\omega) + \frac{\hat{\lambda}(\omega)}{2}}{1 + 2\alpha(\omega - \omega_k)^2} \quad (7)$$

$$\omega_k^{n+1} = \frac{\int_0^\infty \omega |\hat{\mu}_k(\omega)|^2 d\omega}{\int_0^\infty |\hat{\mu}_k(\omega)|^2 d\omega} \quad (8)$$

$$\hat{\lambda}^{n+1}(\omega) \leftarrow \hat{\lambda}^n(\omega) + \tau \left( \hat{x}_f(\omega) - \sum_k \hat{\mu}_k^{n+1}(\omega) \right) \quad (9)$$

where  $\hat{x}_f(\omega)$  is the Fourier transform of the signal  $x_f(t)$ , and  $\hat{\mu}_i(\omega)$  is the Fourier transform of the  $i$ th sub-signals  $\mu_i(t)$ .

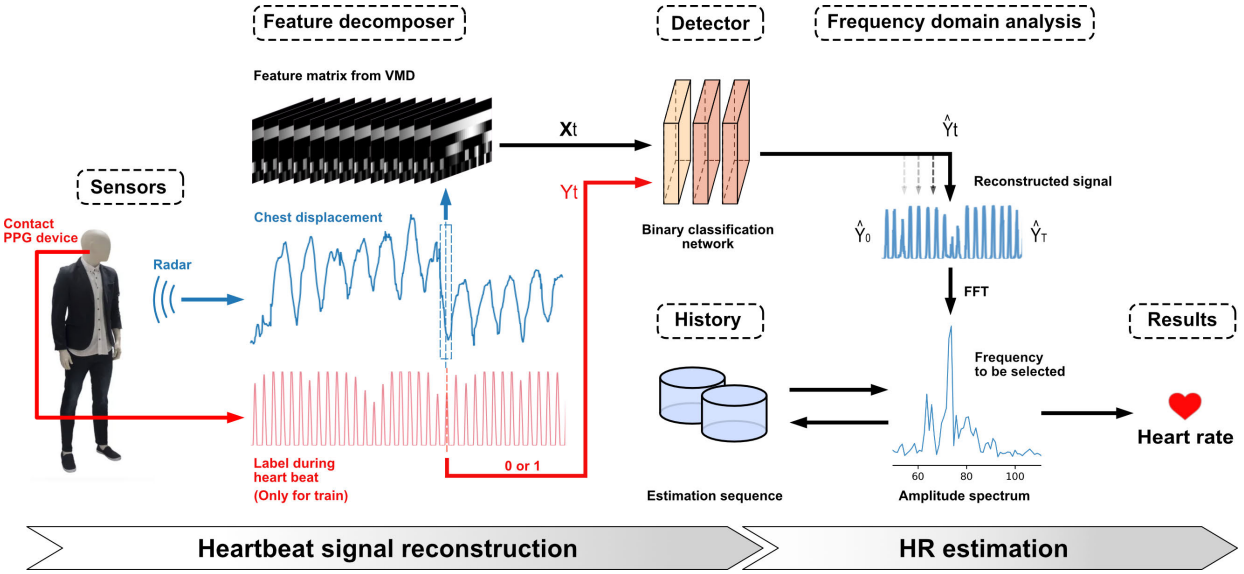


Fig. 7. Signal reconstruction and HR estimation.

The cutoff condition of  $\mu_k$  is as follows:

$$\frac{\sum_k \|\hat{\mu}_k^{n+1} - \hat{\mu}_k^n\|_2^2}{\|\hat{\mu}_k^n\|_2^2} < \varepsilon \quad (10)$$

where  $\varepsilon$  is the tolerance of the convergence criterion (typically around  $10^{-6}$ ).

Fig. 6 shows the results of a typical chest wall displacement decomposed by the VMD algorithm into different independent components, which are ordered from lowest to highest according to their primary frequency. In our proposed method  $\alpha = 2000$  and  $K = 7$ , which is slightly more than that suggested in [27] to ensure adequate decomposition of the original signal. The information in the possible redundant channel can be ignored by the neural network's learning capability.

In the detecting part, we constructed a detector network (binary classification), while the reference value for training is obtained by a time-aligned contact measurement device (PPG). The workflow is shown as Fig. 7. The length of the sliding window is chosen by a priori knowledge of the heartbeat signal periodicity, which in this article is set to 72 frames, corresponding to a time length of about 2 s, to strike a balance between input feature richness and detecting latency. A longer window length facilitates the network to synthesize more information to make more accurate judgments. However, too long windows lead to bigger latency and lower event-time accuracy. Then, the radar data in one sliding window can be shaped as matrix  $\mathbf{X}_t$ , which has a shape of  $7 \times 72$ . The reference label  $\mathbf{y}_t$  is not solely determined by the presence of a heartbeat in the window, but rather by the proximity of the window center  $t$  to the heart beat center  $t_i^{\text{PPG}}$ . Here,  $t_i^{\text{PPG}}$  is extracted from the  $i$ th pulse signal over a threshold from the PPG stream data. If there exists  $t_i^{\text{PPG}}$  to satisfy  $\|t - t_i^{\text{PPG}}\| < \tau$ ,  $\mathbf{y}_t$  is set to True; otherwise, it is set to False.  $\tau$  indicates the expected heartbeat duration and time alignment accuracy, which is set to 8 frames (0.25 s).

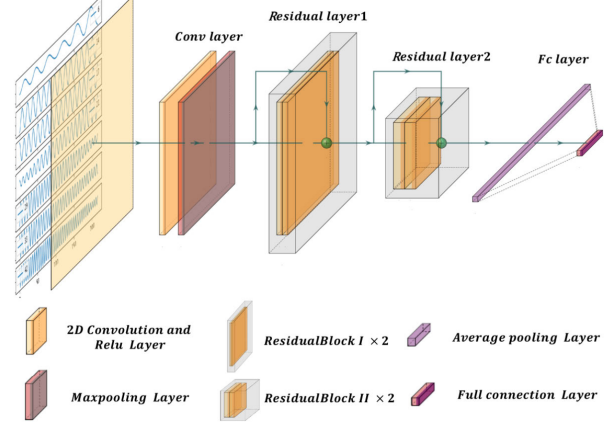


Fig. 8. Architecture of the proposed detector network.

A lightweight neural network serves as the backbone of our detector model. Contrary to normal image classification tasks, the dimension of the input data from the radar is relatively small. Therefore, we constructed a lightweight network based on ResNet [41] as shown in Fig. 8. The detailed model structure is described in Table II. The output of the network is a scalar indicating the probability  $\hat{y}_t = f^{\mathbf{W}}(\mathbf{X}_t) \in \mathbb{R}^1$  that the current window time is a heartbeat moment.  $\mathbf{W}$  note the model parameters (i.e., weights, bias in neural network).

Typically, the optimal parameters are trained by minimizing the binary cross entropy (BCE) loss between the output probability and the reference label from contact heartbeat sensors  $\mathbf{y}$

$$\text{loss}(\mathbf{X}) = -\mathbf{w}[\hat{\mathbf{y}} \cdot \log \mathbf{y} + (1 - \hat{\mathbf{y}}) \cdot \log(1 - \mathbf{y})]. \quad (11)$$

We use an Adam optimizer [42] to update the parameters of the network by maximizing  $\text{loss}(\mathbf{X})$  in (11).

Then, the continuous output as the detected sequence of heartbeat events  $\hat{\mathbf{y}}$  has the same periodicity with the reference heartbeat signal  $\mathbf{y}$  while the sliding window moves. Based on

this primitive thought,  $\hat{y}$  is used as the reconstructed heartbeat signal in the later articles.

### C. HR Estimation

The task of achieving a highly precise frequency estimation in a continuous long-time monitoring process remains challenging. This is due to sudden, significant noise interference that can occur throughout the monitoring process, such as coughing or large random body shakes. To address this issue, we propose to estimate HR by dividing the process into two parts: frequency-domain analysis and correction based on historical data.

Under semi-static conditions, the HR of the human body should not undergo sudden and drastic changes, but instead it should exhibit a smooth and gradual change. Thus, in long-term monitoring scenarios, we can use the historical monitoring information of the same subject from the recent past to determine the reliability of the current monitoring results. While taking into account the randomness of the distribution of noise signals, in most cases the spectral peaks associated with noise are discontinuous in two successive time windows, while the spectral peak associated with HR keeps its location unchanged in several successive time windows.

Similar to some recent studies [30], [43], [44], we established an HR tracking method based on historical information. The spectral peak tracking consists of initialization, peak selection, and verification.

- 1) *Initialization*: In the initialization stage, the subjects are required to reduce body motions as much as possible. Since there is no prior information to help find the correct one, the HR can be estimated by choosing the highest one of the three spectral peaks in reconstructed signal's spectrum during this stage.
- 2) *Peak Selection*: No more than three candidate frequencies with the largest amplitude in the spectrum are selected in the current time windows, of which the amplitude should be no less than a threshold  $\eta$ . In our experiments, the threshold  $\eta$  is set to 85% of the largest amplitude. Denote the candidate frequencies by  $F^i (i = 1, 2, 3)$ , in descending order with related amplitude.
- 3) *Verification*: The first principle is to prevent a large change in the estimated HR values in two successive time windows. Since human HR does not fluctuate dramatically during nonstrengthening activity, the change in HR values within 1 min rarely exceeds 25 beats/min (BPM) [45]. Therefore, the candidate frequency that departs too much from the last previous estimation should be treated as sudden noise and filtered out. Based on the estimated HR previously, the nearest candidate frequency is selected as follows:

$$F_{\text{est}} \leftarrow \arg \min_{F^i} \{|F^i - F_{\text{prev}}|\} \quad (12)$$

where  $F^i$  such that  $|F^i - F_{\text{prev}}| \leq \theta$ , and  $\theta$  notes the defined gap as 25 BPM in our experiments.

If no verified candidate frequency is found, we will opt for the conservative solution to accept the same HR as the

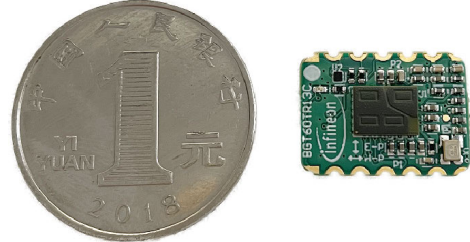


Fig. 9. Infineon BGT60TR13C radar chipset in comparison to one Yuan coin (RMB).

previous historical one as follows:

$$F_{\text{est}} \leftarrow F_{\text{prev}}. \quad (13)$$

The second principle is to prevent from losing tracking over long time. If strong noise interference continues over long time, the same HR selection could happen in many successive time windows. Thus, the spectral peak associated with HR is lost and may not be found back. To avoid this situation, if the previous HR repeats in  $h$  successive time windows, then

$$F_{\text{est}} = F_{\text{prev}} + D_{\text{trend}} \cdot \theta \quad (14)$$

where  $D_{\text{trend}} \in \{-1, 1\}$  indicating the change direction of the HR peak location. In experiments, we set  $h = 3$  and calculated  $D_{\text{trend}}$  as follows:

$$D_{\text{trend}} = \begin{cases} 1, & \text{if } \forall F^i \text{ s.t. } F^i - F_{\text{prev}} > \theta \\ -1, & \text{if } \forall F^i \text{ s.t. } F^i - F_{\text{prev}} < -\theta. \end{cases} \quad (15)$$

## III. EXPERIMENTS

### A. Experiment Setup

*Hardware Implementations*: The proposed HeRe is built on a consumer low-power radar platform for the experimental testing: BGT60TR13C radar chipset from Infineon Technologies AG [46]. It is a power-optimized FMCW radar with AiP resulting in a compact size. As in Fig. 9, the radar chipset is depicted in comparison to one Yuan coin (RMB). This radar has a TX power of just 5 dBm, which is 12.5 times less Tx power than that used in [11], ten times less than that used in [23], and five times less than that used in [10], [22], [24], and [25]. The radar's carrier frequency  $f_c$  is 60 GHz and is configured to send chirps within a frequency range starting from  $f_{\text{min}} = 60$  GHz to  $f_{\text{max}} = 61$  GHz. Thus, a frequency bandwidth  $B = 1$  GHz is covered, which results in a range resolution of  $\delta_r = 15$  cm. Moreover, the radar can send bursts of chirps, which are referred as data frames. However, to minimize power and computational consumption we use the data frame consisting of a single chirp with frame repetition time of 33.3 ms or rate 30 Hz, which is enough for vital signs' monitor. Table III shows the main configuration parameters of the BGT60TR13C radar used for the entire experiments.

During the experiment, the subjects remained still and breathed naturally. As shown in Fig. 10, they were required to wear an on-ear contact PPG sensor to obtain a reference value. Three subjects, who were all between 20 and 30 years old and without heart disease, participated in the experiments for data collection. To evaluate the model's generalizability, only one subject provided the training dataset, while the data

TABLE III  
RADAR CONFIGURATION PARAMETERS

Parameter	Value
Start frequency	60GHz
Stop frequency	61GHz
Bandwidth	1GHz
TX power	5dBm
Duration time of chirp	$137.6\mu s$
Duration time of frame	33.3ms
Frame frequency	30Hz
Chirps in frame	1
Samples in chirp	128
Sample rate	1000Hz

TABLE IV  
DATASET DESCRIPTION

Dataset Type	Dataset Name	Length(Minutes)	Parameters
Training	Single-person	445	Single-person provided, at 0.6m collected
Validation	HR distribution	240	45-90 BPM
	Different distance	80	0.3, 0.6, ..., 2.4 m
	Different subject	45	3 subjects
	Long-duration	240	Continuous monitoring, at 0.6m collected

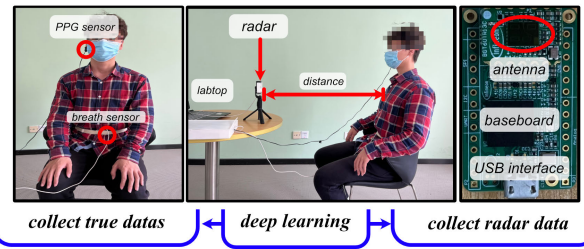


Fig. 10. Experimental setup for mmW radar HR monitoring.

from the other subjects were used to form the validation set. Specifically, we collected 450 min (7.5 h) of monitoring data as the training dataset, which was obtained at a fixed distance of 0.6 m. To assess the proposed method from multiple perspectives, we further obtained 1005 min (16.75 h) of monitoring data as the validation dataset, which was divided into four categories: Datasets with different HR distributions (45–90 BPM), datasets obtained at different distances (0.3–2.4 m), datasets from different subjects (three people), and a long-duration monitoring dataset (240 min). The collected datasets and the relevant parameters are listed in Table IV.

#### B. Time-Domain Analysis

Under low transmit power conditions, various types of noise are the biggest challenge to accurate heartbeat monitoring. For example, random body shaking, object vibrating in the environment, or the noise of the radar circuit itself may generate signals with amplitudes similar or even larger than that of the heartbeat. When the noise signal has similar amplitude and periodicity as the general heartbeat signal, it is difficult to distinguish it effectively by the many of methods proposed in previous works. Fig. 11 shows an example of how the proposed HeRe detects the heartbeats from the

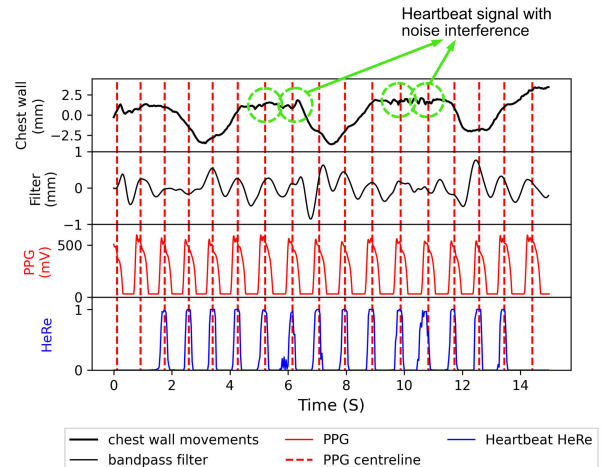


Fig. 11. Illustration of the proposed HeRe for real-time heartbeat detection.

mass of noise signal. The body chest wall movement, the component obtained by HR BPF, the reference PPG signal, and the reconstructed heartbeat signal from HeRe in a 15-s monitor are presented on the same time axis. The red line is the reference signal of the PPG sensor and the center time of the PPG signal corresponding each heartbeat is marked by the red dashed line. Significant noise interference can be seen on the black chest wall displacement signal marked by the green dashed circle. The amplitude and period of the noise have considerable similarity to the heartbeat signal. The blue line shows the reconstructed heartbeat signal given by HeRe. It demonstrates that HeRe successfully distinguishes the real heartbeat from various types of noise. Moreover, the moment of every detected heartbeat is close to those of the reference PPG signal. The slight misalignment that randomly happens is neglectable for heart rate measurement, and it can be explained by the inconsistency in the temporal characteristics of the blood flow and the body vibrations triggered by heartbeat.

#### C. Frequency-Domain Analysis

The original chest wall movement waveform, the chest wall movement waveform through a bandpass filter, and reconstructed heartbeat signal given by HeRe are visualized in the frequency domain as spectrums to investigate the approach's impact for the heartbeat signal.

The original chest wall displacement waveform is displayed in Fig. 12(a), and the respiration component can be observed clearly. Tiny fluctuations in the curve, on the other hand, caused by the heart activity are very weak and almost unnoticeable.

From the amplitude spectrum of the displacement waveform, as shown in Fig. 12(b), it is seen that there are several main peak components in the normal heartbeat frequency range (i.e., 54–96 BPM). The respiration and respiration harmonics are distinct.

The simple FIR bandpass filter (0.8–2 Hz) is carried out, to obtain the heartbeat signal corresponding component signal as shown in Fig. 12(c). Surrounded by noisy peaks, the HR cannot be identified easily in the amplitude spectrum of filtered signal illustrated in Fig. 12(d).

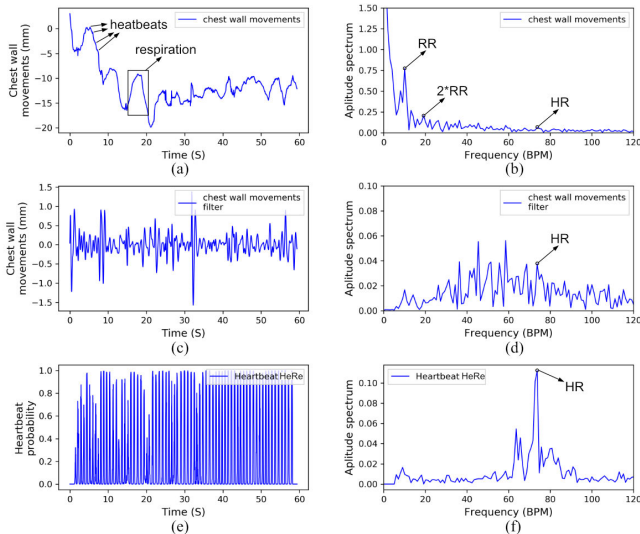


Fig. 12. Illustration of the heartbeat signal enhancement by the proposed HeRe. (a) Chest wall displacement. (b) Amplitude spectrum of the chest wall displacement. (c) Chest wall displacement through a bandpass filter. (d) Amplitude spectrum of the bandpass filtered chest wall displacement. (e) Heartbeat reconstructed signal by HeRe. (f) Amplitude spectrum of the reconstructed heartbeat signal by HeRe.

The reconstructed heartbeat signal based on HeRe and its amplitude spectrum are shown in Fig. 12(e) and (f), respectively. It can be seen that the proposed approach greatly enhances the heartbeat components, and the proportion of the respiration and noise components is greatly reduced.

#### D. Estimation Performance of HR Tracking

Some statistical parameters are defined for the sake of intuition to assess the similarity, robustness, and accurateness of the HeRe method's monitoring results in comparison to other approaches.

The success rate  $P_s$  can be defined as the percentage of that the estimated HR  $F_{\text{est}}(i)$  from the radar within threshold beats  $\Delta F$  of the reference HR  $F_{\text{ref}}(i)$

$$P_s = \frac{\sum_{i=1}^N D[|F_{\text{est}}(i) - F_{\text{ref}}(i)| \leq \Delta F]}{N}$$

$$D[x] = \begin{cases} 1, & \text{if } x \text{ is true} \\ 0, & \text{if } x \text{ is false} \end{cases} \quad (16)$$

where  $N$  stands for the total estimations number, and  $\Delta F$  is set to 4 BPM for heartbeat monitoring in these experiments, indicating the permitted measurement error.

A higher success rate  $P_s$  indicates a better likelihood that the HR estimation error is within the acceptable range. It assesses the acceptability of the HR obtained by the approach.

The mean relative error (MRE) can be calculated by the following:

$$\text{MRE} = \frac{1}{N} \sum_{i=1}^N \frac{|F_{\text{est}}(i) - F_{\text{ref}}(i)|}{F_{\text{ref}}(i)}. \quad (17)$$

MRE represents the relative difference between the measured value and the reference value, and it is an indicator of precision.

And the mean square error (MSE) is also adopted to evaluate estimation's stability, which is defined as

$$\text{MSE} = \frac{1}{N} \sum_{i=1}^N [F_{\text{est}}(i) - F_{\text{ref}}(i)]^2. \quad (18)$$

To assess the efficacy and accuracy of the proposed HeRe approach, we compare it with nine other methods in each categories that have been previously mentioned in Section I. In the category of spectrum analysis methods, the following were selected for comparison: the FFT filtering method [10], the wavelet method [31], and the differential enhancement (DE) method [11]. The FFT filtering method serves as our baseline as it is considered a naive approach. In the category of nonstationary decomposition methods, the following methods were selected: EMD [34], EEMD [24], and VMD [21]. In the category of complex signal processing methods, the following methods were selected: CS-OMP [25], and MRC [26]. These aforementioned methods have been applied on medium-power radar platforms and have achieved good HR monitoring accuracy, which can be considered state-of-the-art. Furthermore, the end-to-end DL-based method in [37] is also performed to evaluate the efficiency of our proposed DL algorithm framework.

The performance evaluation is structured into four parts: Performance 1—various HR distributions, Performance 2—different ranges, Performance 3—different subjects, and Performance 4—long monitoring time (overall evaluation). The proposed method is compared with the spectrum analysis methods in experiments 1, 2, and 3 to demonstrate its effectiveness. In experiment 4, additional comparison methods are introduced, including nonstationary decomposition methods, complex signal processing methods, and DL-based methods, to assess the accuracy level and advancement of the proposed method in relevant work.

1) *Performance 1 (Various HR Distributions):* For the same individual, health status affects the distribution of the individual's mean resting HR. It is important to determine the changes in health status from the changes in mean resting HR over time. To test the ability of our proposed HeRe to monitor HR in different distributions, four validation datasets were selected. Each corresponding continuous monitoring was conducted with a distance of 0.6 m and a monitoring time of 1 h: 45 BPM (low HR state before falling asleep), 60 BPM (resting state), 80 BPM (daily state), and 90 BPM (excited state). The data length of 1 min is taken for each heartbeat rate estimation result.

Fig. 13(a)–(d) shows comparison of the results of HeRe with three other methods mentioned above for heartbeat monitoring in the above four situations with different HR levels, separately. Every figure shows continuous heartbeat monitoring results of 60 min in a single experiment, where the red dashed line represents the heartbeat result predicted by our method, and the black line waveform represents the reference heartbeat result obtained by the PPG sensor. The subject's heartbeat rate swings in the range of 44–110 BPM, and the prediction derived by the approach provided in this work can entirely keep up with the reference value change. Other approaches,

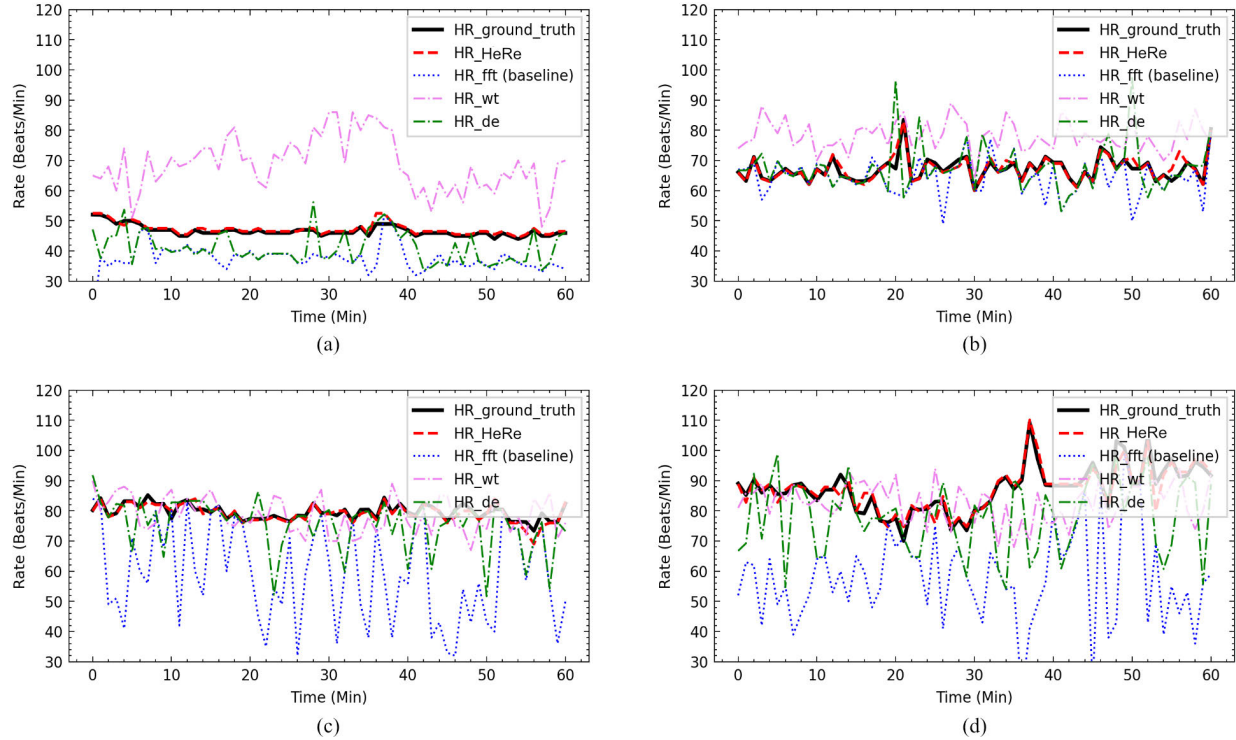


Fig. 13. Comparison result of continuous HR monitoring with different methods for four HR distributions. (a) Mean HR is approximately 45 BPM. (b) Mean HR is approximately 60 BPM. (c) Mean HR is approximately 80 BPM. (d) Mean HR is approximately 90 BPM.

TABLE V  
PERFORMANCE COMPARISON OF DIFFERENT METHODS CORRESPONDING TO THE EXPERIMENTAL RESULTS IN FIG. 13

HR RANGE		45BPM				60BPM				80BPM				90BPM			
Method		MEAN (BPM)	MSE (BPM <sup>2</sup> )	MRE (%)	P <sub>s</sub> (%)	MEAN (BPM)	MSE (BPM <sup>2</sup> )	MRE (%)	P <sub>s</sub> (%)	MEAN (BPM)	MSE (BPM <sup>2</sup> )	MRE (%)	P <sub>s</sub> (%)	MEAN (BPM)	MSE (BPM <sup>2</sup> )	MRE (%)	P <sub>s</sub> (%)
PPG		46.64	-	-	-	67.07	-	-	-	79.6	-	-	-	87.36	-	-	-
HeRe		<b>47.25</b>	<b>0.77</b>	<b>1.43</b>	<b>100</b>	<b>67.27</b>	<b>2.51</b>	<b>1.12</b>	<b>96.7</b>	<b>79.19</b>	<b>1.83</b>	<b>1.1</b>	<b>96.7</b>	<b>87.34</b>	<b>6.78</b>	<b>1.92</b>	<b>90.1</b>
FFT filter [10]		37.42	111.11	19.86	9.8	64.39	47.87	6.5	59	59.27	671.08	25.86	31.1	57.96	1211.66	32.95	9.8
DE [11]		41.13	53.74	13.51	32.7	67.55	67.02	6.68	67.2	75.61	81.56	6.75	67.2	78.09	252.97	12.11	42.6
Wavelet [31]		68.59	561.62	47.17	3.2	78.21	156.92	17.09	9.8	78.62	37.22	6.44	39.3	82.88	123.49	9.58	27.8

on the other hand, can only provide accurate HR estimations on rare occasions due to the low SNR impact of low transmit power radar.

Table V shows comparison of the results of the proposed approach with other methods for heartbeat rate monitoring. The accuracy obtained by the DE approach is somewhat greater than that obtained by the FFT filter and wavelets. All the compared approaches, however, are almost unable to provide reliable HR estimation due to the interference of SNR and respiratory harmonics. The HeRe approach suggested in this article, on the other hand, can successfully counteract the effect of low transmitted power radar on HR tracking, resulting in accurate estimate and lower errors.

2) *Performance 2 (Different Ranges)*: Another well-known fact is that the sensing range affects the estimation accuracy since the radar equation is noted as

$$P_r = \frac{P_t G_t G_r \sigma c^2}{(4\pi)^3 r^4 f_c^2} \quad (19)$$

where  $P_t$ ,  $P_r$  stands for the transmitter (Tx) power and receiver (Rx) power of radar, and  $G_t$ ,  $G_r$  are the antenna gains of the Tx and Rx, respectively. Recall that  $\sigma$  is the target's radar cross section (RCS) and  $r$  is the target range.  $f_c$  is the carrier frequency [47]. The radar echo intensity is inversely

proportional to the 4th power of the distance to the target human body, so that the received SNR decreases sharply as the distance increases.

Therefore, another series of experiments were performed to confirm the stability and reliability of the proposed HeRe along different distances. The target was set at ranges from 0.3 to 2.4 m. Fig. 14 represents the measurement results by four methods at every range, separately.

When the target is located at 0.3 m, the DE and WT methods can also obtain better measurement results because of the high echo SNR, in addition to the proposed method. When the target distance is greater than 0.3 m, the monitoring accuracy obtained by the other compared methods is significantly reduced, except for the proposed method which can maintain a better monitoring result.

Fig. 15 shows the monitoring success rate, mean error, and MSE of the proposed method along with distance. Within 1.2 m, the proposed method is able to obtain 100% monitoring success rate and is able to maintain it above 90% within 1.8 m. Although the MSE increases and the monitoring success rate decreases significantly when the target distance is greater than 1.8 m or more, the average error remains within 10%. During long time monitoring, the average HR monitoring value can be guaranteed to be in a usable state.

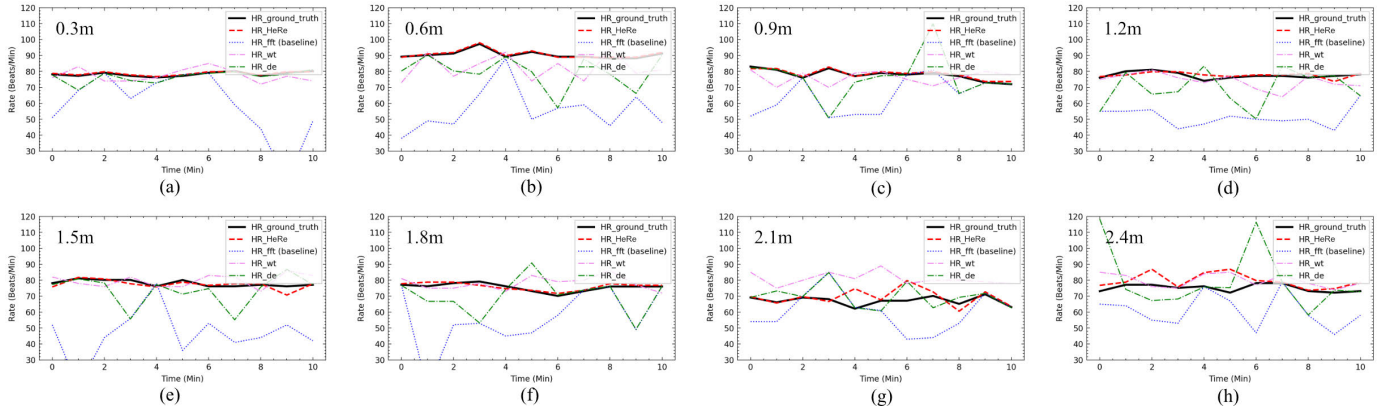


Fig. 14. Comparison result of continuous HR monitoring with different methods for various monitoring distances: (a) at 0.3 m, (b) at 0.6 m, (c) at 0.9 m, (d) at 1.2 m, (e) at 1.5 m, (f) at 1.8 m, (g) at 2.1 m, and (h) at 2.4 m.

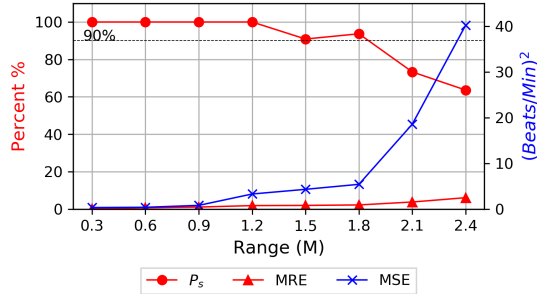


Fig. 15. Performance changes along various monitoring ranges corresponding to the experimental results in Fig. 14.

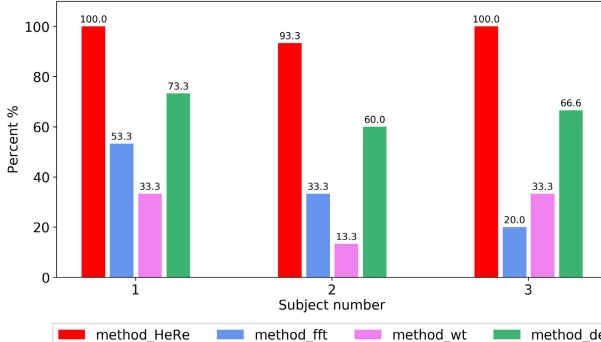


Fig. 16. Success rate of HR estimation result for three participants with four different methods.

3) *Performance 3 (Different Subjects)*: As mentioned previously, the mean resting HR has different distributions when individual differences are considered. In addition, variations in the breathing and heartbeat patterns of various subjects may impact the effectiveness of heartbeat detection. To validate the generalization ability of the proposed neural network model for heartbeat monitoring in the faces of different subjects, three subjects participated in the generalization-validation experiment. For each subject, the HR monitoring lasts 15 min. Fig. 16 depicts the success rate  $P_s$  of HR estimation for each participant using four different methods. In all the cases, the proposed algorithm has a significantly higher detection success rate than the other three, with a success rate greater than 93.3%.

4) *Performance 4 [Long Monitoring Time (Overall Evaluation)]*: A long continuous HR monitoring experiment was

TABLE VI  
PERFORMANCE COMPARISON OF DIFFERENT METHODS CORRESPONDING TO THE LONG CONTINUOUS MONITORING RESULTS IN FIG. 16

Method	MEAN (BPM)	MSE (BPM <sup>2</sup> )	MRE (%)	$P_s$ (%)
PPG	73.54	-	-	-
FFT filtering [10]	63.11	337.51	14.87	50.83
Wavelet [31]	78.34	81.78	10.75	24.16
DE [11]	73.16	42.33	4.8	70.41
EMD [34]	72.14	94.93	8.11	55.41
EEMD [24]	76.04	99.01	8.19	59.58
VMD [21]	72.01	48.59	6.57	56.67
CS-OMP [25]	72.71	43.96	4.76	70.83
MRC [26]	59.11	377.07	19.28	32.92
mBeats [37]	66.29	125.72	11.32	30.42
<b>HeRe</b>	<b>73.42</b>	<b>1</b>	<b>0.62</b>	<b>97.5</b>

conducted to assess the stability of the proposed HeRe approach. The monitoring experiment was conducted for a total of 240 min (4 h), during which the continuity of monitoring was maintained as much as possible except for the subjects' bathroom and meal breaks.

In Fig. 17(a), (c), (e), and (g) the instantaneous HR values of the radar estimating and contacted PPG are compared. The sample points cloud in radar-PPG planes is plotted in Fig. 17(b), (d), (f), and (h), in which the ideal case is all the samples are sitting on the  $y = x$  line, indicating that the radar data are the same as PPG data. Table VI shows comparison of the results of the proposed approach with other methods for long continuous HR monitoring in detail. The results of experiments indicate that the FFT filtering method, which is the baseline, and the MRC method have a low performance in long-time monitoring applications and fail to obtain acceptable measurement accuracy. The data are distributed in a lower HR range (below the  $y = x$  line), which is caused by the unsuppressed harmonic interference of breathing. The EMD method can obtain HR averages closer to the true value; however, the problem of mode aliasing, resulting in adjacent IMF waveforms aliasing and mutual influence, making it difficult to identify, leads to a low monitoring success rate  $P_s$ . To address the modal aliasing issue, we also performed the EEMD method and VMD-based method. The results show that while they are better than the EMD method, they still cannot reach the effect of our proposed method. The DE, CS-OMP, and wavelet methods can obtain HR averages closer

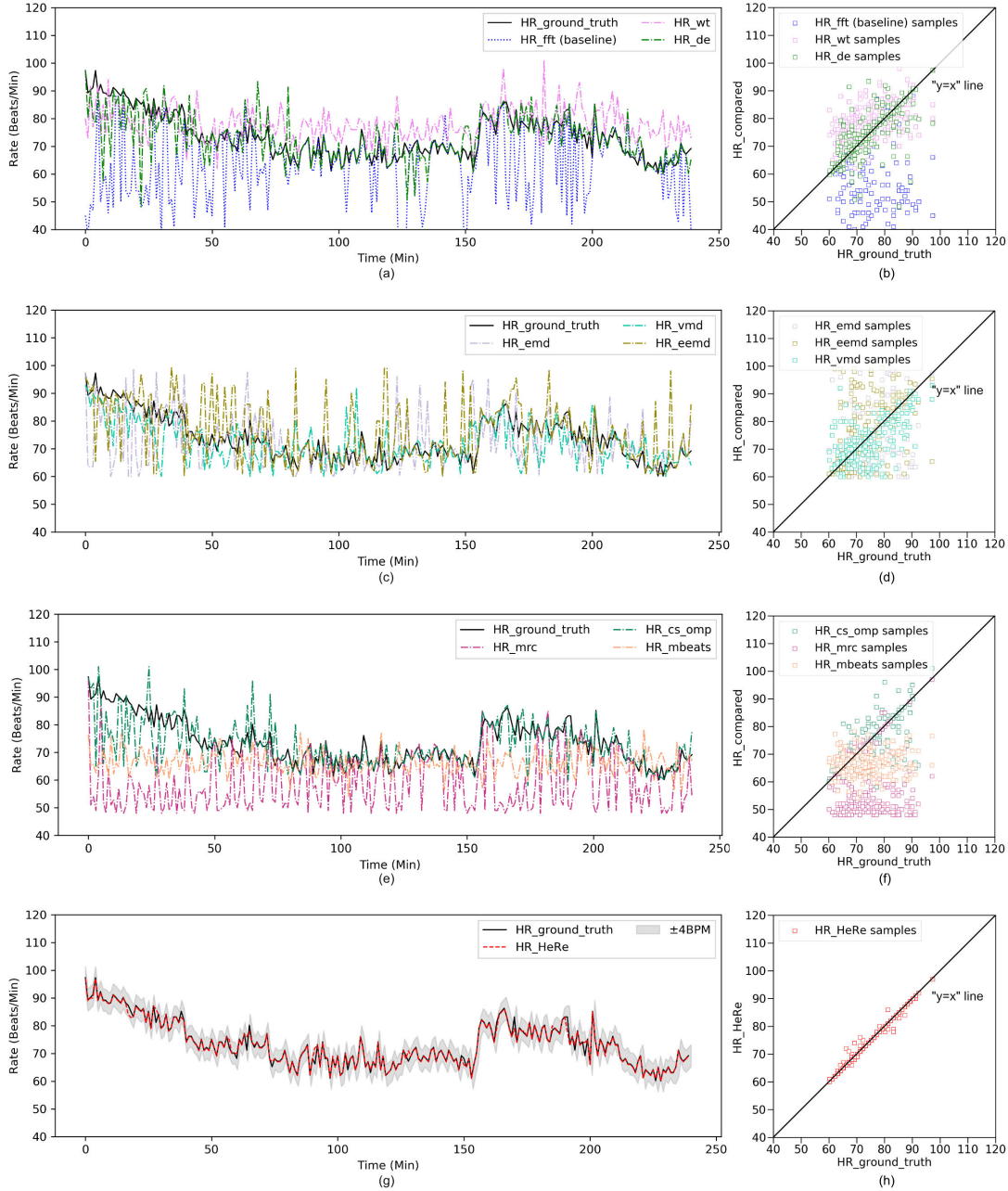


Fig. 17. Long continuous HR monitoring result. (a) HR time trace with the compared methods: FFT filtering, wavelet, and DE. (b) Radar HR with the compared methods (FFT filtering, wavelet, and DE) vs PPG HR. (c) HR time trace with the compared methods: EMD, EEMD, and VMD. (d) Radar HR with the compared methods (EMD, EEMD, and VMD) vs PPG HR. (e) HR time trace with the compared methods: CS-OMP, MRC, and mBeats. (f) Radar HR with the compared methods (CS-OMP, MRC, and mBeats) vs PPG HR. (g) HR time trace with the proposed HeRe. (h) Radar HR with the proposed HeRe vs PPG HR.

to the true value, but their monitoring success rate  $P_s$  is low due to large MSE. They have a poor stability of estimation results. The end-to-end DL method (mBeats) cannot perform well because the learned representations from the end-to-end training approach are unable to transfer nor generalize well when the data are generated with low SNR. In contrast, the HeRe method proposed in this article has better results in all the statistical parameters. As shown in Fig. 17(g), the shaded region representing the zone from the reference HR value of  $\pm 4$  BPM indicates that the majority of samples are within this error, and the success rate  $P_s$  is as high as 97.5% in this 4-h monitoring.

#### IV. CONCLUSION

In this article, we proposed a DL-based signal reconstruction method, HeRe, which transforms the problem of heartbeat signal reconstruction into a signal pattern detection problem. This method enhances the SNR of the heartbeat signal from low-power radar significantly, thus allowing for more precise HR estimation via frequency-domain analysis and the revision of current predictions based on historical data. The high accuracy and robustness could previously only be achieved with high-power radar systems.

We performed several experiments to demonstrate the efficiency of our method in enhancing the heartbeat signal and

to compare it with previous work on practical monitoring, where the method provided a much more accurate estimate. To fulfill the usage scenarios of home monitoring, a series of experiments were performed with different HR distributions, maintaining an accuracy rate above 90% in the common HR ranges. With the lowest 90% accuracy limit, the farthest measurement distance was 1.8 m. When different participants were monitored, the accuracy decreased slightly but still remained above 93.3%, demonstrating its good adaptability to different human bodies. In general, our method is able to achieve the best accuracy in all the cases. We also performed 240 min of long-term HR tracking to demonstrate that our method remained highly stable, with an average accuracy of 97.5%. In addition, since our method does not require any specific qualification of the raw radar data, we believe that the method can be easily adapted to other radar platforms and achieve higher HR monitoring accuracy on high-performance, high SNR radar platforms. The proposed method also has the potential to provide reliable measurements of HR variability (HRV) by identifying individual heartbeat signals, and this issue will be evaluated in a subsequent study.

Despite the fact that the suggested method HeRe provides good HR monitoring accuracy using the present lowest-power mmW radar, there are still significant challenges that must be resolved in the future.

Monitoring vital signs in settings of human mobility is one of the most challenging tasks. The traditional signal processing techniques often fail to effectively eliminate noise produced by small bodily movements, which can be more significant than the chest wall surface vibration caused by breathing and heartbeats. Moreover, due to the variety of motions, it is difficult to represent them using the method presented in this article. Therefore, unsupervised DL methods, which do not require a reference signal for training, show immense potential for our future research, as they can be used to gather training datasets without the need for contact sensors even when the subject is in motion.

The majority of experiments in relevant works are conducted in a laboratory setting with a clearly defined distance. In the home context, other individuals and objects may interfere with the heartbeat signal. It is believed that introducing space perception and beam formation through an MIMO radar system will solve this issue due to its higher angle resolution than conventional mmW radar.

## REFERENCES

- [1] S. Bi, "Cardiac motion monitor based on contact Doppler radar technology," Ph.D. dissertation, Dept. Elect. Comput. Eng., Univ. California, Berkeley, CA, USA, 2018.
- [2] B. P. Yan et al., "High-throughput, contact-free detection of atrial fibrillation from video with deep learning," *JAMA Cardiology*, vol. 5, no. 1, p. 105, Jan. 2020.
- [3] Z. Yue, S. Ding, S. Yang, L. Wang, and Y. Li, "Multimodal information fusion approach for noncontact heart rate estimation using facial videos and graph convolutional network," *IEEE Trans. Instrum. Meas.*, vol. 71, pp. 1–13, 2022.
- [4] M. Mercuri, Y.-H. Liu, I. Lorato, T. Torfs, A. Bourdoux, and C. van Hoof, "Frequency-tracking CW Doppler radar solving small-angle approximation and null point issues in non-contact vital signs monitoring," *IEEE Trans. Biomed. Circuits Syst.*, vol. 11, no. 3, pp. 671–680, Jun. 2017.
- [5] C. Gu, Z. Peng, and C. Li, "High-precision motion detection using low-complexity Doppler radar with digital post-distortion technique," *IEEE Trans. Microw. Theory Techn.*, vol. 64, no. 3, pp. 961–971, Mar. 2016.
- [6] E. Piuzzi, P. D'Atanasio, S. Pisa, E. Pittella, and A. Zambotti, "Complex radar cross section measurements of the human body for breath-activity monitoring applications," *IEEE Trans. Instrum. Meas.*, vol. 64, no. 8, pp. 2247–2258, Aug. 2015.
- [7] X. Hu and T. Jin, "Short-range vital signs sensing based on EEMD and CWT using IR-UWB radar," *Sensors*, vol. 16, no. 12, p. 2025, 2016.
- [8] E. Schires, P. Georgiou, and T. S. Lande, "Vital sign monitoring through the back using an UWB impulse radar with body coupled antennas," *IEEE Trans. Biomed. Circuits Syst.*, vol. 12, no. 2, pp. 292–302, Apr. 2018.
- [9] L. Anitori, A. de Jong, and F. Nennie, "FMCW radar for life-sign detection," in *Proc. IEEE Radar Conf.*, May 2009, pp. 1–6.
- [10] M. Alizadeh, G. Shaker, J. C. M. De Almeida, P. P. Morita, and S. Safavi-Naeini, "Remote monitoring of human vital signs using mm-wave FMCW radar," *IEEE Access*, vol. 7, pp. 54958–54968, 2019.
- [11] Y. Xiong, Z. Peng, C. Gu, S. Li, D. Wang, and W. Zhang, "Differential enhancement method for robust and accurate heart rate monitoring via microwave vital sign sensing," *IEEE Trans. Instrum. Meas.*, vol. 69, no. 9, pp. 7108–7118, Sep. 2020.
- [12] D. Zito et al., "SoC CMOS UWB pulse radar sensor for contactless respiratory rate monitoring," *IEEE Trans. Biomed. Circuits Syst.*, vol. 5, no. 6, pp. 503–510, Dec. 2011.
- [13] J. Wang, X. Wang, Z. Zhu, J. Huangfu, C. Li, and L. Ran, "1-D microwave imaging of human cardiac motion: An ab-initio investigation," *IEEE Trans. Microw. Theory Techn.*, vol. 61, no. 5, pp. 2101–2107, May 2013.
- [14] Z. Yang, P. H. Pathak, Y. Zeng, X. Liran, and P. Mohapatra, "Monitoring vital signs using millimeter wave," in *Proc. 17th ACM Int. Symp. Mobile Ad Hoc Netw. Comput.* New York, NY, USA: Association for Computing Machinery, Jul. 2016, pp. 211–220.
- [15] A. De Groot, M. Wantier, G. Cheron, M. Estenne, and M. Paiva, "Chest wall motion during tidal breathing," *J. Appl. Physiol.*, vol. 83, pp. 1531–1537, Nov. 1997.
- [16] *Nest Hub (2nd Gen)*. Accessed: Apr. 24, 2023. [Online]. Available: [https://store.google.com/ca/product/nest\\_hub\\_2nd\\_gen?hl=en-GB](https://store.google.com/ca/product/nest_hub_2nd_gen?hl=en-GB)
- [17] J. Lien et al., "Soli: Ubiquitous gesture sensing with millimeter wave radar," *ACM Trans. Graph.*, vol. 35, no. 4, p. 142, Jul. 2016.
- [18] Aqara. *Human Existence Sensor FPI | Aqara Green M Whole House Intelligence*. Accessed: Sep. 20, 2022. [Online]. Available: [https://www.aqara.com/cn/Aqara-Presence-Detector-FPI\\_overview](https://www.aqara.com/cn/Aqara-Presence-Detector-FPI_overview)
- [19] G. Matthews, B. Sudduth, and M. Burrow, "A non-contact vital signs monitor," *Crit. Rev. Biomed. Eng.*, vol. 28, nos. 1–2, pp. 173–178, 2000.
- [20] M. Sekine and K. Maeno, "Non-contact heart rate detection using periodic variation in Doppler frequency," in *Proc. IEEE Sensors Appl. Symp.*, Feb. 2011, pp. 318–322.
- [21] C. Ding, J. Yan, L. Zhang, H. Zhao, H. Hong, and X. Zhu, "Noncontact multiple targets vital sign detection based on VMD algorithm," in *Proc. IEEE Radar Conf. (RadarConf)*, May 2017, pp. 0727–0730.
- [22] Q. Huang, D. Lu, J. Hu, H. Fan, M. Liang, and J. Zhang, "Simultaneous location and parameter estimation of human vital sign with MIMO-FMCW radar," in *Proc. IEEE Int. Conf. Signal, Inf. Data Process. (ICSIDP)*, Dec. 2019, pp. 1–4.
- [23] H. Lee, B.-H. Kim, J.-K. Park, and J.-G. Yook, "A novel vital-sign sensing algorithm for multiple subjects based on 24-GHz FMCW Doppler radar," *Remote Sens.*, vol. 11, no. 10, p. 1237, 2019.
- [24] L. Sun et al., "Remote measurement of human vital signs based on joint-range adaptive EEMD," *IEEE Access*, vol. 8, pp. 68514–68524, 2020.
- [25] Y. Wang, W. Wang, M. Zhou, A. Ren, and Z. Tian, "Remote monitoring of human vital signs based on 77-GHz mm-wave FMCW radar," *Sensors*, vol. 20, no. 10, p. 2999, 2020.
- [26] T. K. V. Dai et al., "Enhancement of remote vital sign monitoring detection accuracy using multiple-input multiple-output 77 GHz FMCW radar," *IEEE J. Electromagn., RF Microw. Med. Biol.*, vol. 6, no. 1, pp. 111–122, Mar. 2022.
- [27] X. Zhang, Z. Liu, Y. Kong, and C. Li, "Mutual interference suppression using signal separation and adaptive mode decomposition in noncontact vital sign measurements," *IEEE Trans. Instrum. Meas.*, vol. 71, 2022, Art. no. 4001015.
- [28] FC Commission et al., "Code of federal regulations," Federal Commun. Commission, Washington, DC, USA, Tech. Rep. 47 CFR 15.255 (Code of Federal Regulations, Title 47, Part 15, Section 15.255), 2005.

- [29] M. Arsalan, A. Santra, and C. Will, "Improved contactless heartbeat estimation in FMCW radar via Kalman filter tracking," *IEEE Sensors Lett.*, vol. 4, no. 5, pp. 1–4, May 2020.
- [30] W. Zhang, G. Li, Z. Wang, and H. Wu, "Non-contact monitoring of human heartbeat signals using mm-wave frequency-modulated continuous-wave radar under low signal-to-noise ratio conditions," *IET Radar, Sonar Navigat.*, vol. 16, no. 3, pp. 456–469, Mar. 2022.
- [31] C. Bae, S. Lee, and Y. Jung, "High-speed continuous wavelet transform processor for vital signal measurement using frequency-modulated continuous wave radar," *Sensors*, vol. 22, no. 8, p. 3073, Apr. 2022.
- [32] G. Mauro, M. De Carlos Diez, J. Ott, L. Servadei, M. P. Cuellar, and D. P. Morales-Santos, "Few-shot user-adaptable radar-based breath signal sensing," *Sensors*, vol. 23, no. 2, p. 804, Jan. 2023.
- [33] M. Nosrati and N. Tavassolian, "Accuracy enhancement of Doppler radar-based heartbeat rate detection using chest-wall acceleration," in *Proc. IEEE Int. Microw. Biomed. Conf. (IMBioC)*, Philadelphia, PA, USA, Jun. 2018, pp. 139–141.
- [34] F. Weishaupt, I. Walterscheid, O. Biallawons, and J. Klare, "Vital sign localization and measurement using an LFMCW MIMO radar," in *Proc. 19th Int. Radar Symp. (IRS)*, Bonn, Germany, Jun. 2018, pp. 1–8.
- [35] W. Wang et al., "Feasibility study of practical vital sign detection using millimeter-wave radios," *CCF Trans. Pervasive Comput. Interact.*, vol. 3, no. 4, pp. 436–452, Nov. 2021.
- [36] T. Sakamoto and K. Yamashita, "Noncontact measurement of autonomic nervous system activities based on heart rate variability using ultra-wideband array radar," *IEEE J. Electromagn., RF Microw. Med. Biol.*, vol. 4, no. 3, pp. 208–215, Sep. 2020.
- [37] P. Zhao et al., "Heart rate sensing with a robot mounted mmWave radar," in *Proc. IEEE Int. Conf. Robot. Autom. (ICRA)*, May 2020, pp. 2812–2818.
- [38] F. Adib, H. Mao, Z. Kabelac, D. Katahi, and R. C. Miller, "Smart homes that monitor breathing and heart rate," in *Proc. 33rd Annu. ACM Conf. Human Factors Comput. Syst.*, Apr. 2015, pp. 837–846.
- [39] K. Dragomiretskiy and D. Zosso, "Variational mode decomposition," *IEEE Trans. Signal Process.*, vol. 62, no. 3, pp. 531–544, Feb. 2014.
- [40] D. P. Bertsekas, *Constrained Optimization and Lagrange Multiplier Methods*. New York, NY, USA: Academic, May 2014.
- [41] K. He, X. Zhang, S. Ren, and J. Sun, "Deep residual learning for image recognition," in *Proc. IEEE Conf. Comput. Vis. Pattern Recognit. (CVPR)*, Dec. 2015, pp. 770–778.
- [42] D. P. Kingma and J. Ba, "Adam: A method for stochastic optimization," 2014, *arXiv:1412.6980*.
- [43] Z. Zhang, Z. Pi, and B. Liu, "TROIKA: A general framework for heart rate monitoring using wrist-type photoplethysmographic signals during intensive physical exercise," *IEEE Trans. Biomed. Eng.*, vol. 62, no. 2, pp. 522–531, Feb. 2015.
- [44] M. Mercuri, I. R. Lorato, Y.-H. Liu, F. Wieringa, C. Van Hoof, and T. Torfs, "Vital-sign monitoring and spatial tracking of multiple people using a contactless radar-based sensor," *Nature Electron.*, vol. 2, pp. 252–262, Jun. 2019.
- [45] N. B. Taylor, "Voluntary acceleration of the heart," *Amer. J. Physiol.-Legacy Content*, vol. 61, no. 3, pp. 385–398, Aug. 1922.
- [46] IT AG. *BGT60TR13C | XENSIV<sup>®</sup> 60 GHz Radar Sensor for Advanced Sensing—Infineon Technologies*. Accessed: Sep. 27, 2022. [Online]. Available: <https://www.infineon.com/cms/en/product/sensor/radar-sensors/radar-sensors-for-iot/60ghz-radar/bgt60tr13c/>
- [47] S. Schellenberger, K. Shi, F. Michler, F. Lurz, R. Weigel, and A. Koelpin, "Continuous in-bed monitoring of vital signs using a multi radar setup for freely moving patients," *Sensors*, vol. 20, no. 20, p. 5827, Oct. 2020.



**Fuchuan Du** received the bachelor's degree in mechanical engineering from Shanghai Jiao Tong University, Shanghai, China, in 2021, where he is currently pursuing the master's degree with the State Key Laboratory of Mechanical System and Vibration, School of Mechanical Engineering.

His current research interests include utilization of millimeter-wave radar for healthcare.



**Hao Zhu** received the bachelor's degree in mechanical engineering from Shanghai Jiao Tong University, Shanghai, China, in 2021, where he is currently pursuing the master's degree with the State Key Laboratory of Mechanical System and Vibration, School of Mechanical Engineering.

His current research interests include utilization of millimeter-wave radar for healthcare.



**Zhuangzhuang Zhang** received the B.S. degree from Northwestern Polytechnical University, Xi'an, China, in 2018. He is currently pursuing the Ph.D. degree with the School of Mechanical Engineering, Shanghai Jiao Tong University, Shanghai, China.

His research interests include smart sensing, multimodal reinforcement learning, and representation learning.



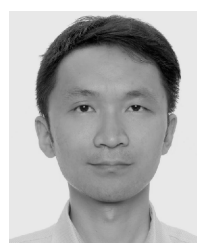
**Yizhao Wang** received the B.S. degree in mechanical engineering and automation from Shandong University, Jinan, China, in 2018. He is currently pursuing the Ph.D. degree with the School of Mechanical Engineering, Shanghai Jiao Tong University, Shanghai, China.

His research interests include smart sensing, visual simultaneous localization and mapping (SLAM), and visual place recognition.



**Qixin Cao** received the Ph.D. degree in agricultural machinery engineering from Kagoshima University, Kagoshima, Japan, in 1997.

He is currently a Professor with the State Key Laboratory of Mechanical System and Vibration, School of Mechanical Engineering, Shanghai Jiao Tong University, Shanghai, China. His current research interests include ubiquitous robotics, intelligent sensing and 3-D environment modeling technology, intelligent robotics and modular technology, and intelligent maintenance and the Internet-of-Things technology.



**Xiaoxiao Zhu** received the B.S. and M.S. degrees in mechanical engineering from the Nanjing University of Aeronautics and Astronautics, Nanjing, China, in 2004 and 2007, respectively, and the Ph.D. degree in engineering from Shanghai Jiao Tong University, Shanghai, China, in 2014.

He is currently a Research Associate with the Student Innovation Center, Shanghai Jiao Tong University. His current research interests include vibration analysis, robotics, robot localization, and smart factory.



**Haili Wang** received the bachelor's degree from the Beijing Institute of Technology, Beijing, China, in 2016, and the master's degree in mechatronics and robotics technology from the Bauman Moscow State Technical University, Moscow, Russia, in 2019. He is currently pursuing the Ph.D. degree with the State Key Laboratory of Mechanical System and Vibration, School of Mechanical Engineering, Shanghai Jiao Tong University, Shanghai, China.

His current research interests include signal processing, vibration analysis, and microwave sensing, in particular for noncontact vital signs' acquisition using radar systems.